Supporting information

Nanoscale coherent interface strengthening of Mg alloys

Qiuming Peng*[,1], Bingcheng Ge[1], Hui Fu[1], Yong Sun[1], Qun Zu[2], Jianyu Huang[1]

[1]*State Key Laboratory of Metastable Materials Science and Technology, Yanshan University, Qinhuangdao 066004, China.*

[2] *School of Mechanical Engineering, Hebei University of Technology, Tianjin 300401, China.*

**Correspondence to: pengqiuming@ysu.edu.cn*

Supplementary content

S.1 Microstructure of the pristine Mg-13 Li alloy

The microstructure has been investigated by high-resolution transmission electron microscopy (HRTEM), where some black particles (~20 nm) are homogeneously distributed in the alloy (**Fig. S1a**). The elemental composition has been confirmed by an electron energy loss spectrometer (EELS) (**Fig. S1b**). The black dot is assigned to Mg-rich phase (α phase, 10.65 and 21.55 eV), while the matrix corresponds to the β phase (7.5 and 22.5 eV). HRTEM images (**Figure S1c-e)** show that the spacing parameters of hcp Mg-rich phase are 3.322 and 5.362 Å. The spacing of bcc Li-rich phase is ~3.677 Å. The deviation from theoretical values is related to solid-solution alloying elements. In addition, the crystalline coherent relationship between bcc Li-rich phase and hcp Mg-rich phase is confirmed by selected area electron diffraction**,** in which the relationship can be shown as following: $(110)_{\beta}//(0001)_{Mg;}$ $(1\bar{1}0)_{\beta}//(01\bar{1}0)_{Mg}$ and $[001]//[2\bar{1}\bar{1}0]$. It clarifies that the as-cast Mg-13Li alloy is also composed of duplex structure instead of traditional simple phase [S1] (β phase).

S.2 Process of ultrahigh pressure treatment

The purity binary Mg-13 Li alloy with a low impurity concentration of ~1wt.% (**Table S1**) was performed. The material preparation and ultrahigh pressure (UHP, over 1GPa for metals) procedures were performed. The pristine as-cast Mg-13Li alloy is used as a reference. The high pressure process can be divided into three stages. Firstly, the exterior pressure was loaded. Then the temperature was increased to certain value. Finally, the temperature remained for 30 min. After high temperature treatment, the pressure was unloaded immediately, and the samples were rapidly cooled to room temperature.

S.3 Movies

Movie S1. Nucleation and growth of $\{10\bar{1}1\}$ twin in perfect Mg. Under $[1\bar{2}10]$ direction tension, the initial plastic deformation begins with the nucleation of a $\{10\bar{1}1\}$ twin at the strain of 0.0746 in Mg single crystal. Then a secondary $\{10\bar{1}2\}$ twin follows the primary

twin, combining into a $\{10\bar{1}1\}-\{10\bar{1}2\}$ double twin structure. The interface between the two reoriented crystals shows a zigzag characteristic consisting of co-existing $\{10\bar{1}2\}$ twin boundary (TB) and basal/prismatic (BP) interface. With the increasing strain, the reoriented crystals grow gradually and basal SFs nucleate in the reoriented crystals. And then the annihilation of $\{10\bar{1}2\}$ twin lattice can be observed due to the migration of $\{10\bar{1}2\}$ TB and BP interface, leaving a coarse $\{10\bar{1}1\}$ twin at the strain of 0.079.

Movie S2. Stacking faults affect the formation of {10$\bar{1}$1} twin. To study the effect of SFs on the nucleation and growth of $\{10\bar{1}1\}$ twin, two basal SFs were pre-implanted in the Mg single crystal by superposing the anisotropic elastic displacement fields [S2], evenly dividing the model into three parts. The twin preferentially nucleates in the junction of surface and SF under $[1\bar{2}10]$ direction tension, and grows towards two sides, forming multi-crystals. Meanwhile, numbers of basal SFs can form in the reoriented crystals. Compared with the simulation in perfect Mg, the $\{10\bar{1}1\}$ twin nucleation in this model accompanies with the lower yield stress and strain. Furthermore, the growth of twins was limited by the interaction of multiple interfaces.

Movie S3. Dislocation escape in the pyramidal plane. Taking a screw dislocation as an example, the pre-implanted dislocation will spontaneously escape from the pyramidal plane during the relaxation process, suggesting the strengthening role is weak.

Movie S4. Dislocation pinning by SFs. To study the effect of SF on the dislocation movement, a SF and a prism <a> dislocation were created in the Mg single crystal by superposing the anisotropic elastic displacement fields [S2]. A uniaxial compression loading was exerted along $[1\bar{2}10]$ direction so as to activate the dislocation movement.

Supplementary references

(S1) Wu, S. K.; Chien, C.; Yang, C. S.; Bor, H. Y. The Portevin-Le Chatelier effect in β-phase Mg-14.3 Li-0.8 Zn alloy.*Mater. Sci. Eng. A* **2014,** *605,* 33-38.

(S2) Barnett, D.M.; Lothe J. An image force theorem for dislocations in anisotropic bicrystals. *J. Phys. F. Met. Phys.* 1974, **4**, 1618-1621.

Supporting table

Table S1. Chemical composition of the as-cast Mg-13Li alloy.

Sample	Composition (wt.%)						
	Li	Zn	Al	Fe	Cu	Ni	Mg
Mg-13Li	12.55	0.12	0.81	0.0366	0.0055	<0.001	Balance

Supporting figures.

Figure S1. Microstructure of the as-cast Mg-13Li alloy. (**a**) TEM image of the as-cast Mg-13Li sample. (**b**) EELS maps of the particles and matrix. (**c**) HRTEM image of Li-rich particles with bcc structure along [001] direction. (**d**) HRTEM image of Mg-rich matrix with hcp structure along [01 $\bar{1}$1] direction. (**e**) SAED pattern of the sample. The coherent crystalline relationship is detected.

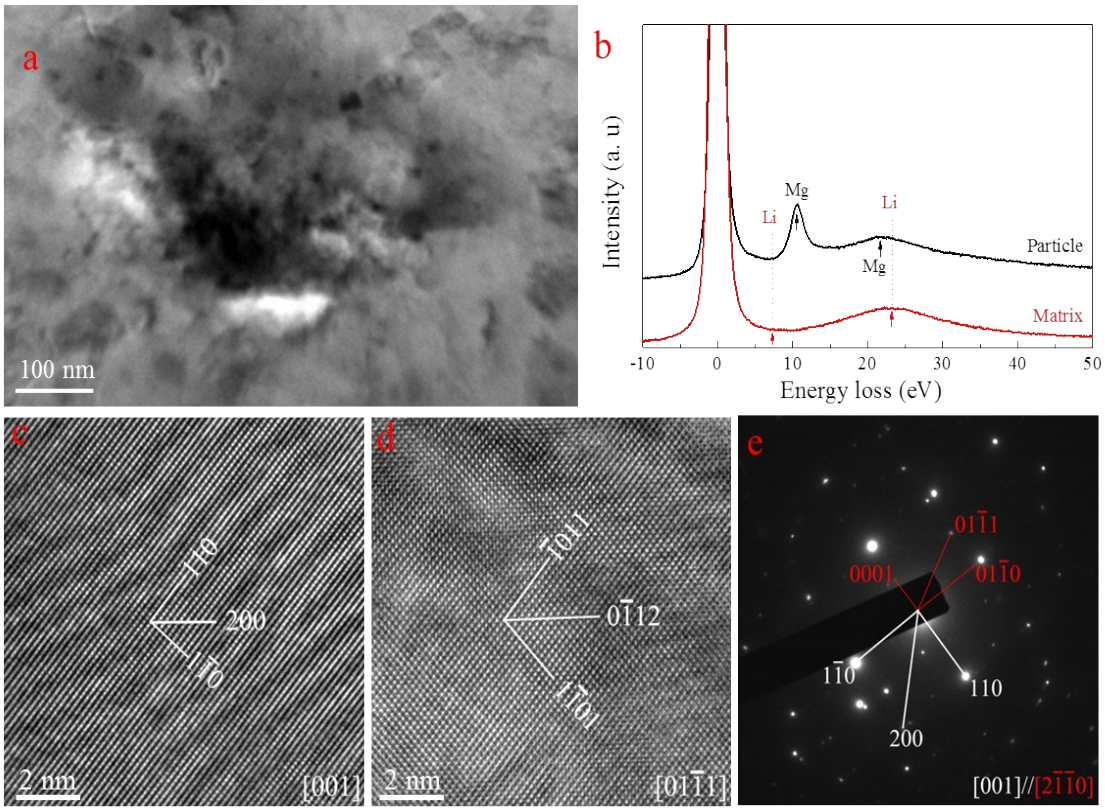

Figure S2. (a) The average spacing of SFs calculated based on 50 random twins. The SFs-T corresponds to the SFs in the interior of nanotwins. The SFs-M corresponds to the SFs in the matrix. (b) The HRTEM of SFs in TBs. The two separated partial SFs were terminated in TBs.

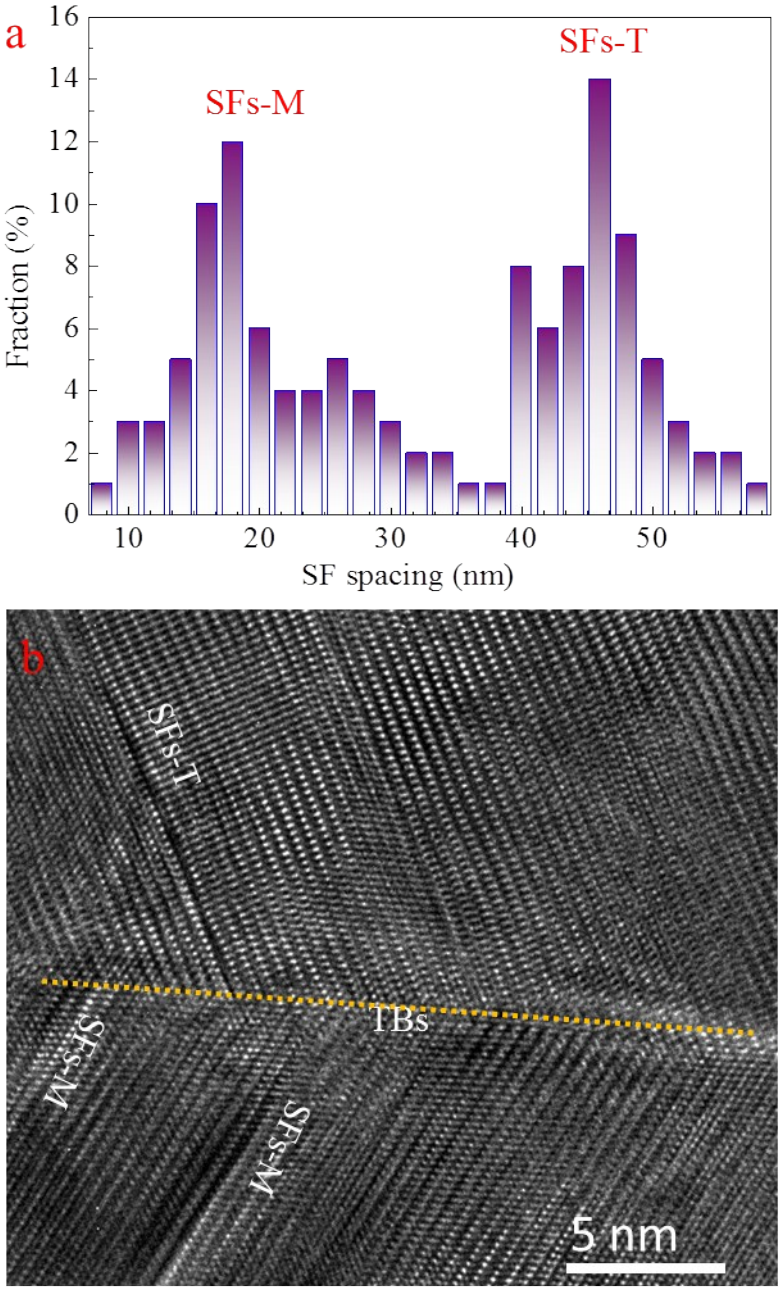

Figure S3 (a) Mircrohardness dependent on the different high pressure conditions. (**b**) Tensile properties of different state UHPed Mg-13Li alloys with an initial strain rate of 1.7×10^{-3} s^{-1}. (**c**) Compressive properties of different state UHPed Mg-13Li alloys with an initial strain rate of 1.7×10^{-3} s^{-1}.

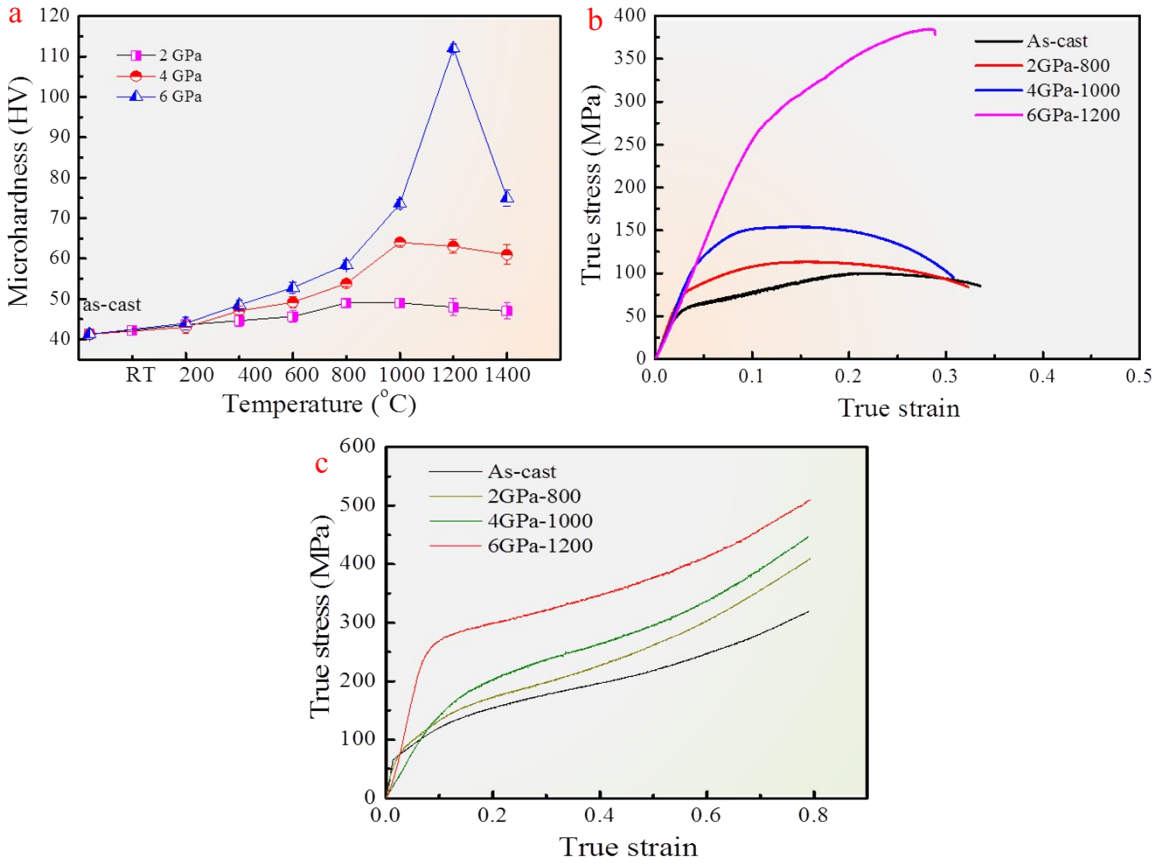

Figure S4. Typical morphologies of the different samples before (**a**) and after (**b**) tensile testing. Typical morphologies of the different samples before (**c**) and after (**d**) compressive testing.

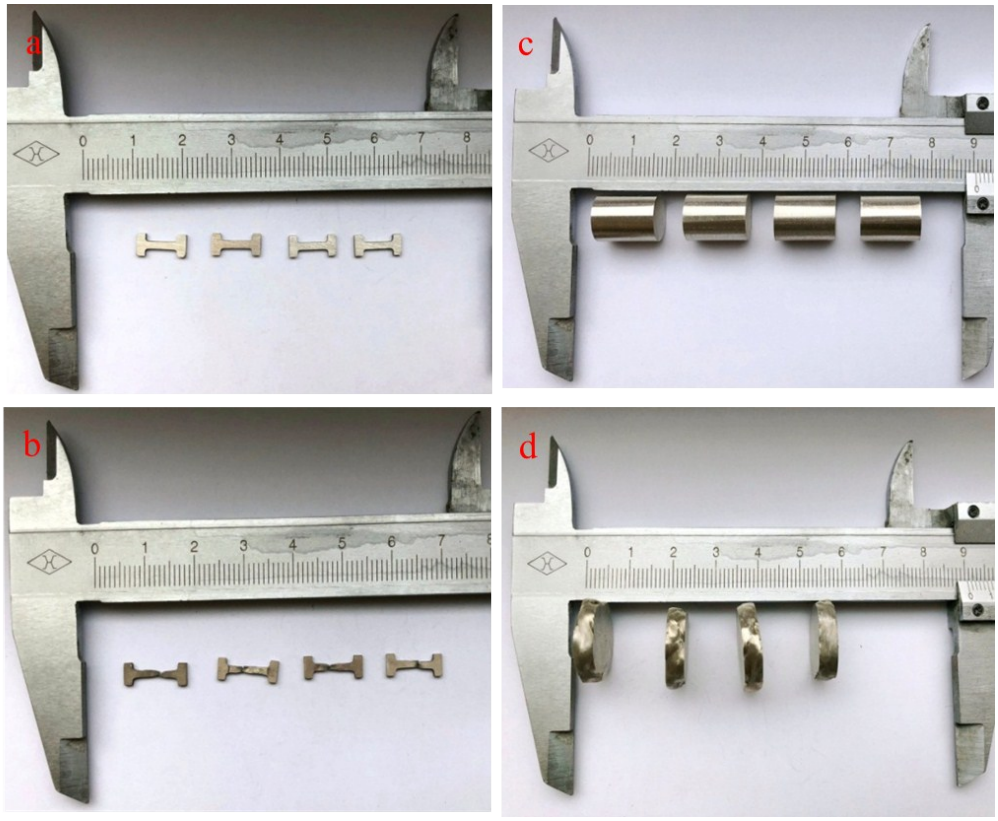

Figure S5. (**a**) TEM image of the 6GPa-1200 Mg-13Li alloy with a true strain of 0.1.The severe deformed microstructure is confirmed (white triangles). (**b**) A HRTEM image of TBs. The Burgers circuit shows Frank partial dislocation is pinned along TBs.

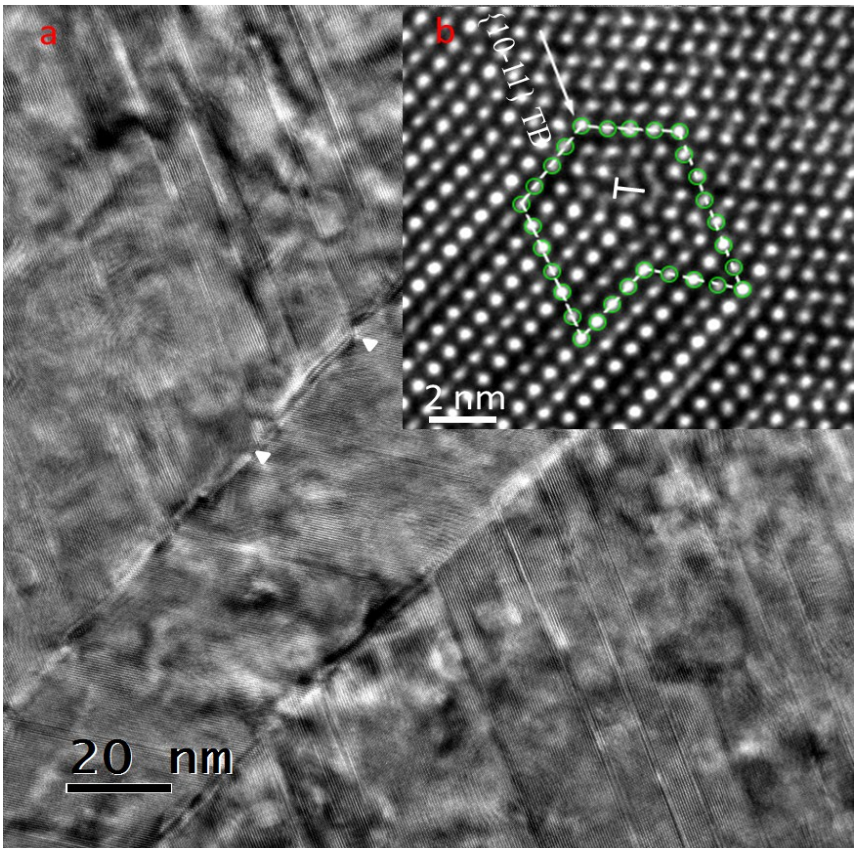

Figure S6. HRTEM of TBs in 6GPa-1200 Mg-8Li alloy with a true strain of 0.1. The serrated-shaped steps with the heights of 16, 8 and 4 atomic-layer steps (ALs) are observed.